Microgravity Science and Technology (2020) 32:1185–1197
https://doi.org/10.1007/s12217-020-09841-9

ORIGINAL ARTICLE

Effects of Gravitational Force and Surface Orientation on the Jumping Velocity and Energy Conversion Efficiency of Coalesced Droplets

Xin Wang[1] · Bo Xu[1,2,3] · Zhenqian Chen[1,2,3] · Yang Yang[4] · Qian Cao[4]

Received: 19 June 2020 / Accepted: 6 October 2020 / Published online: 30 October 2020

Abstract

Due to potential applications in numerous fields (self-cleaning, anti-frosting, condensation enhancement, etc.), coalescence-induced droplet jumping has been investigated extensively by numerical simulations and experiments over the past decade. In this paper, the jumping dynamics of coalesced droplets on the microstructured superhydrophobic surfaces is simulated using the lattice Boltzmann model. Effects of gravity, inclined angle and droplet radius ratio on the jumping velocity and energy conversion efficiency are studied. The numerical results demonstrate that jumping droplets on inclined surfaces driven by the tangential gravity can successfully detach from the surface without returning to the original spot. The jumping velocity can be improved by a larger inclined angle. Coalescence-induced jumping of two-mismatched droplets on the horizontal surface can also produce a horizontal velocity that drives them detaching from the surface along x direction or coalescing with other droplets. Both jumping velocity and energy conversion efficiency are reduced by a lower radius ratio and a larger gravitational coefficient. In addition, no jumping behavior can be observed when energy conversion efficiency is less than 2%.

Keywords Lattice Boltzmann method · Inclined angle · Gravity · Droplet jumping

This article belongs to the Topical Collection: The Effect of Gravity on Physical and Biological Phenomena
Guest Editor: Valentina Shevtsova

Highlights
(1) Droplet jumping dynamics on microstructured and inclined surfaces is simulated.
(2) Jumping droplets driven by tangential gravity can detach from the surface without returning.
(3) Effect of gravity on the jumping behavior should be considered.
(4) No jumping behavior can be observed when energy conversion efficiency is less than 2%.

✉ Zhenqian Chen
zqchen@seu.edu.cn

[1] School of Energy and Environment, Southeast University, Nanjing, People's Republic of China

[2] Jiangsu Provincial Key Laboratory of Solar Energy Science and Technology, School of Energy and Environment, Southeast University, Nanjing, People's Republic of China

[3] Key Laboratory of Energy Thermal Conversion and Control of Ministry of Education, School of Energy and Environment, Southeast University, Nanjing, People's Republic of China

[4] Engineering and technology center for space applications, Chinese academy of sciences, Beijing, People's Republic of China

Introduction

The phenomena of self-propelled droplet movement have attracted much attention in recent years due to the potential applications in the fields of self-cleaning (Wisdom et al. 2013), anti-icing (Boreyko and Collier 2013; Xu et al. 2014), defrosting (Chu et al. 2017; Hou et al. 2018) microfluidic systems (Wang et al. 2018a; Chen and Deng 2017) and enhanced condensation heat transfer (Xu and Chen 2019; Wang et al. 2020; Xie et al. 2019), etc. It has been demonstrated that surface energy is released after droplet coalescence and excess kinetic energy drives droplets jumping from the surface. During dropwise condensation, coalescence-induced microdroplet jumping is superior to gravity-driven droplet rolling, which greatly reduces the renewal time of supercooled surface to enhance dropwise condensation heat transfer (Wen et al. 2018; Wen et al. 2019). Several organisms can remove the dust adhering to the surface by means of droplet jumping to accomplish self-cleaning effect (Barthlott and Neinhuis 1997). Therefore, an in-depth understanding of self-propelled jumping behavior induced by coalescence is of great value for engineering application.

Since coalescence-induced jumping of condensate droplets was firstly reported by Boreyko and Chen (Boreyko and Chen 2009), a large number of experimental investigations in recent years have been carried out on the jumping behavior induced by condensate droplets. Miljkovic et al. (2013) designed and prepared a copper-based superhydrophobic surface and found that compared with conventional hydrophobic surface, heat transfer coefficient during jumping-microdroplet condensation can be increased by 30% at low supersaturations. Kim et al. (2015) found that jumping velocity of multi-droplet coalescence can be increased by 50% compared with double droplets, which improves the condensation performance by 40%. Cha et al. (2016) studied coalescence-induced nanodroplet jumping on superhydrophobic surface with carbon nanotubes, indicating that critical jumping radius increases with increasing solid fraction and decreasing apparent advancing angle. Non-ideal surface interactions and droplet morphology play crucial roles in limiting the minimum radius of jumping droplets. In addition, several experimental work of coalescence-induced droplet jumping under non-condensing conditions by microscopic visualization technology was also conducted. Effects of droplet numbers, size distribution, surface wettability and surface structure on the jumping velocity and jumping height were analyzed (Wang et al. 2017a, b; Yan et al. 2019). However, due to the tiny droplet size and extremely short jumping time, it is difficult to accurately record the entire jumping process using existing microscopic visualization techniques. Furthermore, arbitrary droplet size and distribution arrangement are also challenges for experiment.

With the rapid improvement of computational efficiency, numerical simulation has become an effective tool in multiphase flow and has been successfully applied to the droplet dynamics (Shi et al. 2019; Li et al. 2016; Zhang et al. 2019; Xie et al. 2016; Xu and Chen 2018). Researchers conducted large quantities of numerical work on the coalescence-induced droplet jumping dynamics because of the controllable droplet size, arbitrary distribution arrangement and adjustable surface wettability. Liu et al. (Liu et al. 2014a) simulated identical double-droplets coalescing on a superhydrophobic surface with $\theta = 180°$ using 3D phase field model and predicted the jumping velocity accurately. Cheng et al. (Cheng et al. 2016) reported that contact angle hysteresis (CAH) has a significant effect on the droplet jumping through transient 3D diffuse interface method. The higher advancing angle and lower receding angle contribute to improving the jumping velocity. Yuan et al. (Yuan et al. 2019) used the 3D VOF method to simulate the coalesced droplet jumping on superhydrophobic surface with wettability gradient. The results indicated that surface energy gradient reduces the symmetry of the coalesced droplets, thus reducing the energy conversion efficiency. Also, effects of droplet size, distribution arrangement, liquid density, surface wettability and surface roughness on the jumping velocity were analyzed by lattice Boltzmann (LB) method (Liu and Cheng 2015; Shi et al. 2015; Farokhirad et al. 2015; Wang et al. 2017b; Wang et al. 2019) and the corresponding jumping velocities were successfully predicted. However, there are few investigations on the effects of surface orientation and initial radius ratio on the jumping velocity and energy conversion efficiency. It was demonstrated by Mukherjee et al. (Mukherjee et al. 2019) that the jumping droplets will return to the horizontal surface and eventually be pinned on the substrate, while the jumping droplets will successfully detach from the inclined surface driven by gravity. Mismatched droplets coalescence would reduce the jumping velocity and energy conversion efficiency (Yan et al. 2019). In addition, effect of gravitational field is also supposed to be taken into account compared with viscous dissipation and energy dissipation induced by drag force when the capillary length and droplet size are on the same order of magnitude.

In this paper, LB model is used to simulate the dynamic behaviors of coalescence-induced droplet jumping. Effects of gravity, radius ratio and surface orientation on the jumping velocity and energy conversion efficiency are analyzed. This work will expand our understanding of the mechanism of coalesced droplet jumping.

Model Description

LB Pseudopotential Model

In the LB model, the fluid is characterized and described by the particle distribution function, which is evolved on the

specific lattice. The evolution equation of fluid particle distribution function using BGK collision operator is written as:

$$f_\alpha(\mathbf{x}+\mathbf{e}_\alpha\delta_t, t+\delta_t)-f_\alpha(\mathbf{x},t) = -\frac{1}{\tau_f}\left[f_\alpha(\mathbf{x},t)-f_\alpha^{eq}\left(\mathbf{x},t\right)\right]+\Delta f_\alpha(\mathbf{x},t) \quad (1)$$

where $f_\alpha(\mathbf{x}, t)$ represents the distribution function of fluid particles at the lattice site $\mathbf{x}$ and time t and τ_f is the dimensionless relaxation time. The implementation of evolution equation can be divided into two steps:

$$\text{Collision step}: f_\alpha'(\mathbf{x},t) = f_\alpha(\mathbf{x},t)-\frac{1}{\tau_f}\left[f_\alpha(\mathbf{x},t)-f_\alpha^{eq}\left(\mathbf{x},t\right)\right]+\Delta f_\alpha(\mathbf{x},t) \quad (2a)$$

$$\text{Convection step}: f_\alpha(\mathbf{x}+\mathbf{e}_\alpha\delta_t, t+\delta_t) = f_\alpha'(\mathbf{x},t) \quad (2b)$$

where $f_\alpha'(\mathbf{x}, t)$ is the distribution function after collision. $\Delta f_\alpha(\mathbf{x}, t)$ is the force term, including fluid-fluid force, fluid-solid force and gravitational force, etc. The equilibrium distribution function $f_\alpha^{eq}(\mathbf{x}, t)$ is given by:

$$f_\alpha^{eq} = \omega_\alpha\rho\left[1+\frac{\mathbf{e}_\alpha\cdot\mathbf{u}}{c_s^2}+\frac{(\mathbf{e}_\alpha\cdot\mathbf{u})^2}{2c_s^4}-\frac{\mathbf{u}^2}{2c_s^2}\right] \quad (3)$$

D2Q9 discrete velocity model is adopted with the weight coefficients of $\omega_0 = 4/9$, $\omega_{1-4} = 1/9$ and $\omega_{5-8} = 1/36$, written as:

$$\mathbf{e}_\alpha = \begin{bmatrix} 0 & 1 & 0 & -1 & 0 & 1 & -1 & -1 & 1 \\ 0 & 0 & 1 & 0 & -1 & 1 & 1 & -1 & -1 \end{bmatrix} \quad (4)$$

The density and velocity of fluid can be obtained from the statistics of the distribution function:

$$\rho = \sum_\alpha f_\alpha, \mathbf{u} = \sum_\alpha \mathbf{e}_\alpha f_\alpha / \sum_\alpha f_\alpha \quad (5)$$

Through multi-scale analysis of Champman-Enskog expansion, discrete lattice Boltzmann equation can be restored to macroscopic Navier-Stokes equation, and the fluid kinematic viscosity can be expressed as:

$$\upsilon = c_s^2\left(\tau_f-0.5\right)\delta_t \quad (6)$$

The introduction method of force term has a great impact on the numerical precision and stability of LB model. On account of independent of relaxation time and better numerical stability, force term is directly added to the particle distribution function using exact difference method (EDM) (Gong and Cheng 2012):

$$\Delta f_\alpha(\mathbf{x},t) = f_\alpha^{eq}(\rho(\mathbf{x},t), \mathbf{u}+\Delta\mathbf{u})-f_\alpha^{eq}(\rho(\mathbf{x},t), \mathbf{u}) \quad (7)$$

where $\Delta\mathbf{u} = F\cdot\delta_t/\rho$ is the velocity change caused by the total force during the unit time step. In this paper, the total force $\mathbf{F}$ is composed of the fluid-fluid force $\mathbf{F}_{\text{int}}$, fluid-solid force $\mathbf{F}_s$ and gravitational force $\mathbf{F}_g$, written as:

$$\mathbf{F}_{\text{int}} = -\beta\psi(x)\sum_\alpha G(\mathbf{x}+\mathbf{e}_\alpha)\psi(\mathbf{x}+\mathbf{e}_\alpha)\mathbf{e}_\alpha - \frac{1-\beta}{2}\sum_\alpha G(\mathbf{x}+\mathbf{e}_\alpha)\psi^2(\mathbf{x}+\mathbf{e}_\alpha)\mathbf{e}_\alpha \quad (8a)$$

$$\mathbf{F}_s(\mathbf{x}) = -G_s\psi(\mathbf{x})\sum_\alpha\omega_\alpha S_{\omega i}(\mathbf{x}+\mathbf{e}_\alpha\delta_t) \quad (8b)$$

$$\mathbf{F}_g(\mathbf{x}) = (\rho(\mathbf{x})-\rho_v)\mathrm{g} \quad (8c)$$

where ψ is the interaction potential function, $\psi(\mathbf{x}) = \sqrt{2(p-\rho c_s^2)}/g_0$. The pressure p can be obtained from the actual equation of state (EOS). Here, Peng-Robinson (P-R) equation of state is chosen:

$$p = \frac{\rho RT}{1-b\rho}-\frac{a\rho^2\alpha(T)}{1+2b\rho-b^2\rho^2} \quad (9)$$

where $\alpha(T) = [1+(0.37464+1.54226\omega-0.26992\ \omega^2)\left(1-\sqrt{T/T_{cr}}\right)]^2$ and $\omega = 0.344$, $a = 2/49$, $b = 2/21$, $R = 1$.

After obtaining the total force, the true fluid velocity $\mathbf{U}$ is defined as the average velocity before and after collision:

$$\rho\mathbf{U} = \rho\mathbf{u}+0.5\delta_t\mathbf{F} \quad (10)$$

Computational Domain and Dimension Conversion

In this paper, a 601 × 501 lattice structure is chosen to be the two-dimensional computational domain. The half way bounce-back scheme is adopted at the solid wall and periodic boundary conditions are employed at other boundaries. The gas and liquid densities are 7.2 and 0.197, respectively, which is in good agreement with the theoretical analysis of Maxwell construction. According to Eq. (6), the viscosity ratio between liquid and gas is $\upsilon_l / \upsilon_v = 36.5$. Here, $(\rho_l+\rho_v)/2$ is defined as the gas-liquid interface. Initially, two droplets with a tiny distance are placed on the solid surface. Then, coalescing and jumping behavior of droplets can be seen caused by the released surface energy. Driven by tangential component of gravity, coalesced droplet will jump off the original spot, as shown in Fig. 1(a). After two mismatched droplets coalescence, jumping droplet will also produce a little distance due to the asymmetry (Fig. 1b). The letters a, s and h are used to denote the width, spacing and height of micropillar arrays, respectively.

To be compared with other published experimental and numerical data, it is necessary to convert the lattice units into dimensionless units. Liu et al. (2014b) reported that lattice units can be related to physical units by the dimensionless Ohnesorge (Oh) number. The Oh number is a dimensionless criterion number, which represents the relationship between viscous force and inertial force and surface tension, defined as:

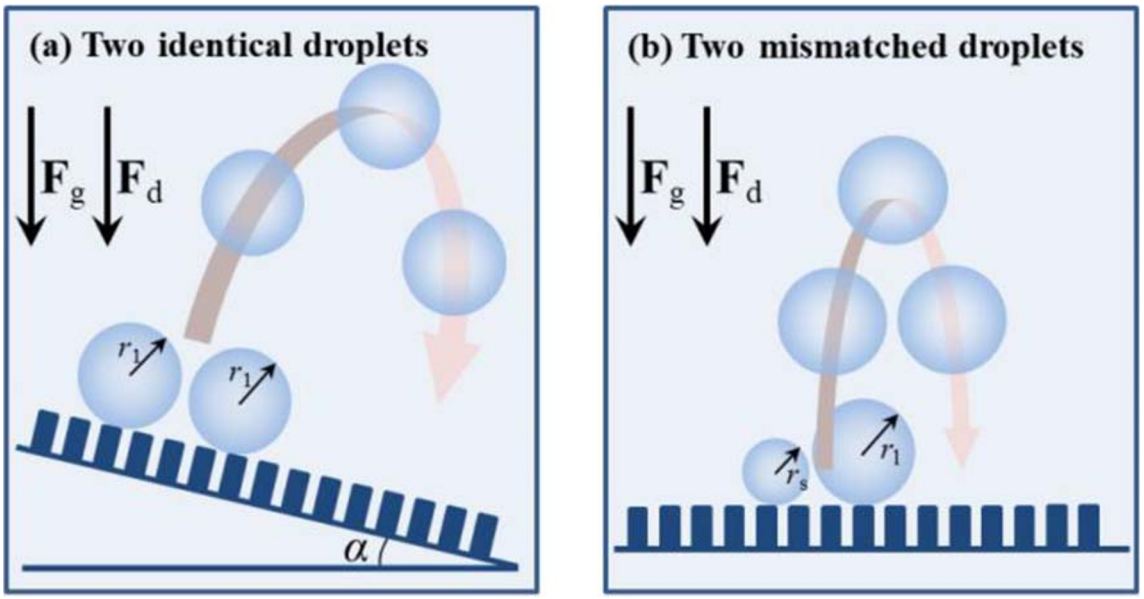

Fig. 1 Schematic diagram of coalescence-induced droplet jumping: (**a**) two identical droplets and (**b**) two mismatched droplets

$$Oh = \mu_l / \sqrt{\rho_l \sigma_{lv} r_l} \tag{11}$$

Herein, the initial droplet size can be represented by *Oh* number because viscosity, density and surface tension are all constants. And lattice time is non-dimensionalized with inertia-capillary time:

$$t^* = t / \sqrt{\rho r_l^3 / \sigma_{lv}} \tag{12}$$

The jumping velocity is defined as the ratio of mass-averaged velocity to inertia-capillary velocity:

$$v^* = \frac{\int_V \rho_l v dV}{\int_V \rho_l dV} \sqrt{\frac{\rho_l r_0}{\sigma_{lv}}} \tag{13}$$

where V represents the area occupied by the liquid.

Verification of our LB Results with Previous Experimental and Numerical Data

Figure 2 shows the comparison of our LB results with published experimental and numerical data. Although superhydrophobic surfaces in experiments of Khatir et al. (2016) ($\theta = 157°$) and Yan et al. (2019) ($\theta = 169°$) are rough, roughness factor (RF) is so tiny that it can be considered as smooth surfaces. The results show that their jumping velocities are larger at the same *Oh* number, as shown in Fig. 2. Jumping velocities in our LB simulation are slightly lower than those of Wang's (Wang et al. 2017b) but higher than Liu's (Liu et al. 2014a). As shown in Table 1, superhydrophobic surfaces with $\theta = 160°$ in Wang's model are homogeneous, whereas the surfaces are microstructured in our simulation ($a = 3.2$ μm, $s = 8.1$ μm, $h = 16.2$ μm, $\theta = 166°$) and Liu's model ($a = 1.3$ μm, $s = 5.3$ μm, $h = 10.7$ μm, $\theta = 165°$). It has been indicated that jumping velocity of coalesced droplet is reduced by microstructured surface because it penetrates into the pocket during coalescence, thus increasing the energy dissipation. Comparison of the above results, we conclude that the jumping velocities in our simulation agree well with other published data. Therefore, coalescence-induced droplet jumping behavior can be predicted accurately using our LB model.

Results and Discussion

Two Identical Droplets

Generally, coalescence-induced droplet jumping can be divided into four stages: (I) liquid bridge formation after coalescence; (II) liquid bridge expanding and impacting the solid substrate; (III) retraction caused by the wall reaction and (IV) jumping off the surface. Figure 1 shows the dynamic evolution of coalescence-induced droplet jumping on horizontal and inclined surfaces ($r_1 = 48.6$ μm, $Oh = 0.017$). Width, spacing and height of micropillar arrays are $a = 3.2$ μm, $s = 22.7$ μm and $h = 24.3$ μm, respectively. And the corresponding static contact angle is 166°. Initially, two identical droplets with a tiny distance are placed on the surface. Quickly, they merge to form a liquid bridge, suspended on the micropillar arrays, which corresponds to Stage (I). With the liquid bridge expanding, coalesced droplet impinges the micropillars. It can be seen that a little portion of droplet enters the air pocket between the micropillars at $t^* = 1.091$ (Stage II). As the droplet is counteracted by the solid wall, it begins to retract toward the center and contact area between droplet and substrate

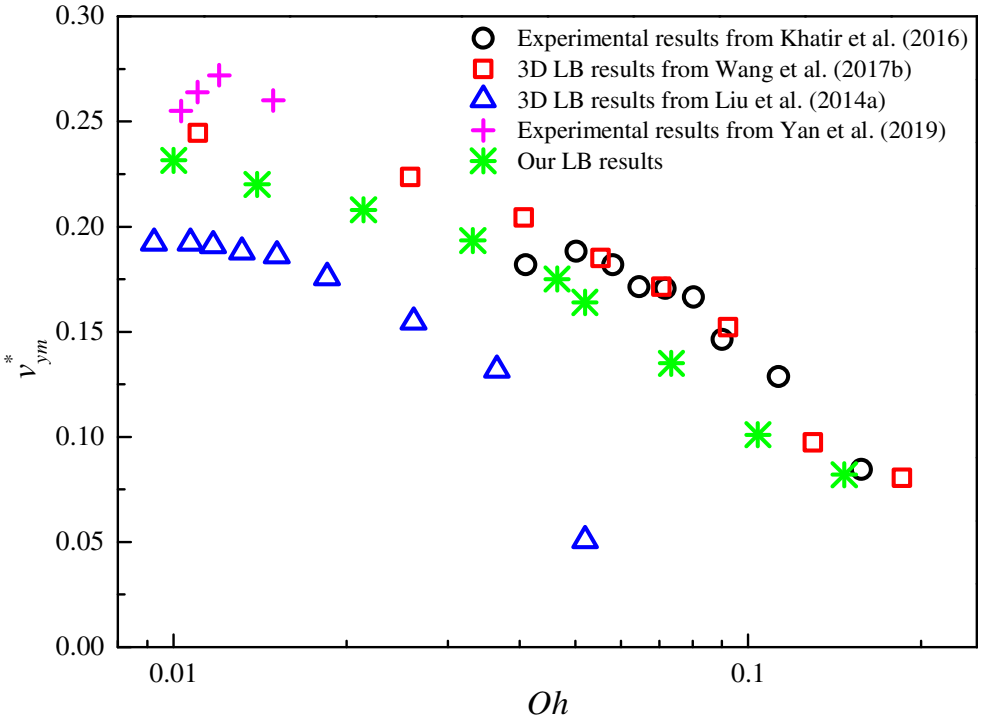

Fig. 2 Comparison of our LB results with published experimental and numerical data

decreases (Stage III). Eventually, the drop jumps off the surface due to the remnant kinetic energy (Stage IV). Comparing Fig. 3(a) with Fig. 3(b), we conclude that inclined angle has little effect on the first three stages but has a significant influence on stage IV in the whole jumping process. For horizontal surface, jumping droplet will return to the origin spot in the absence of tangential driving force, which causes an additional thermal resistance during dropwise condensation or even damages the micropillar structure resulting in the superhydrophobicity failure. In contrast, the drop on inclined surfaces can successfully detach from the surface without returning driven by the tangential component of gravity.

In order to better understand the influence of inclined angle and gravity on jumping velocity, variation of jumping velocity with time under two different gravitational coefficients of $g = 0.1 \times 10^{-7}$ and $g = 10 \times 10^{-7}$, as plotted in Fig. 4. The inclined angles are 15°, 30°, 45°, 60° and 75°, respectively. When coalescing on the solid surface, the droplets are mainly governed by the viscous force, resistance caused by the contact angle hysteresis and gravity. After jumping from the surface, it is affected by drag force and gravitational force. When two droplets merge under lower gravitational coefficient ($g = 0.1 \times 10^{-7}$), the tangential component of gravity is less compared with the viscous force and is sufficient to drive the droplet to move along x-axial direction at a speed of $\sim 10^{-3}$. According to our statistics, tangential velocity changes intricately in the first three stages, while it increases steadily with time in Stage IV. A larger inclined angle has a positive effect on increasing tangential velocity. At early time (from Stage I to Stage II), formed liquid bridge has a tendency to impact the solid substrate, with the vertical jumping velocity reducing to a negative value. During retraction (Stage III), vertical jumping velocity increases rapidly to the maximum due to the reaction of substrate. Eventually, it slowly decreases under the action of drag force after jumping off the surface. As can be seen from the enlarged figure, vertical velocity difference is no more than 1%, indicating that inclined angle has no effect on the jumping velocity at lower gravitational coefficient ($g = 0.1 \times 10^{-7}$). In contrast, inclined angle has a conspicuous influence on jumping velocity at higher gravitational coefficient ($g = 10 \times 10^{-7}$). The tangential velocity increases linearly with time, at which point tangential component of gravity plays a dominant role compared with viscous force. The greater the inclined angle, the larger the tangential velocity is, which is due to the greater tangential gravity. As the inclined angle increases, the tangential accelerations are 0.00432, 0.00836,

Table 1 Experimental and numerical conditions from different references

References	Method	θ	CAH	Surface
(Khatir et al. 2016)	Experiment	157°	4°	Rough, RF<<r
(Wang et al. 2017b)	LBM	160°	/	Smooth
(Liu et al. 2014a)	LBM	165°	/	Rough
(Yan et al. 2019)	Experiment	169°	2.6°	Rough, RF<<r
This paper	LBM	166°	/	Rough

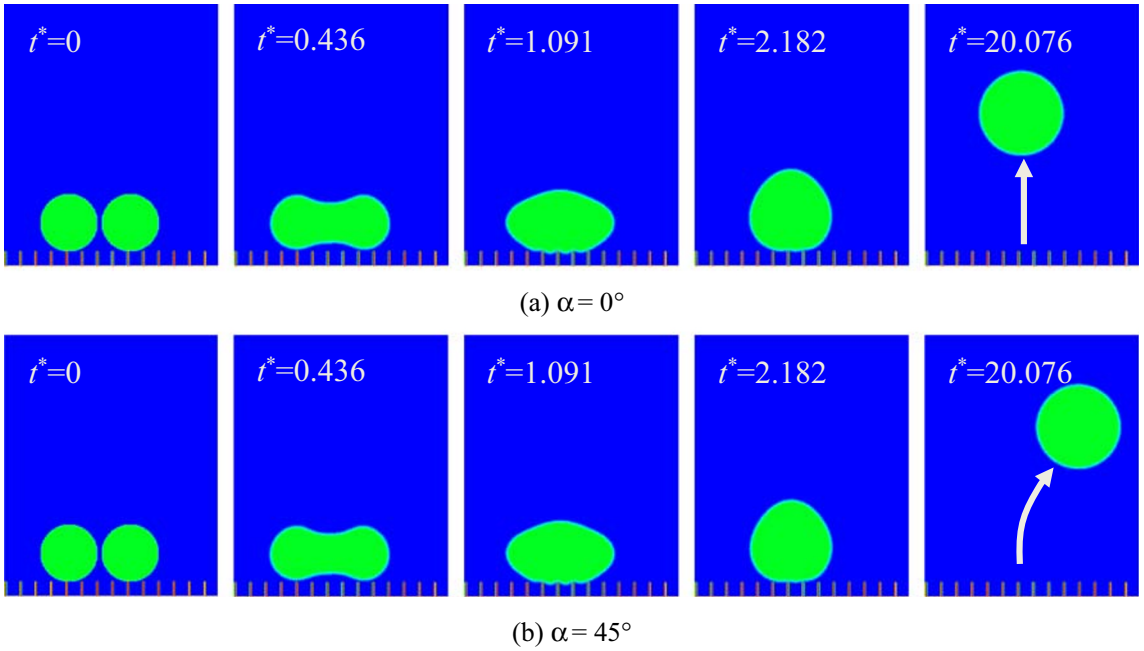

Fig. 3 Dynamic evolution of coalescence-induced droplet jumping on horizontal and inclined surfaces ($Oh = 0.017$, $\theta = 166°$, $g = 5 \times 10^{-7}$). (**a**) $\alpha = 0°$, (**b**) $\alpha = 45°$

0.01184, 0.01453, and 0.01623, respectively. For $g = 10 \times 10^{-7}$, a larger inclined angle increases the peak vertical velocity and reduces the decrease rate of vertical velocity in Stage IV.

Figure 5 shows the effect of gravitational coefficient on maximum vertical velocity of jumping droplet ($Oh = 0.017$). As can be seen from Fig. 4, maximum vertical velocity appears in Stage III (droplet retraction before detaching from the surface). In this simulation, the parameters including surface wettability and micropillar structure are the same. Bond (Bo) number denoting the relative importance of gravity and surface tension is used to represent effect of gravity field on maximum jumping velocity:

$$Bo = \rho_l g r_1^2 / \sigma_{lv} \tag{14}$$

It is found from Fig. 5 that maximum jumping velocity decreases with an increasing Bo number, and the decreasing rate is significantly accelerated. When the Bo number is relatively lower, inclined angle has little effect on maximum jumping velocity. As Bo number increases, the difference between maximum jumping velocities increases at various inclined angles. When the relative difference between maximum jumping velocities on different inclined surfaces is greater than 1% ($\varepsilon = \frac{\left[\left(v_{ym}^*\right)_{\max} - \left(v_{ym}^*\right)_{\min}\right]}{\left(v_{ym}^*\right)_{\max}} \times 100\% \geq 1\%$), the gravitational force should be taken into account. Taking $r_1 = 48.6$ μm as an example, the relative difference of maximum jumping velocity is $1.4\% > 1\%$ at $Bo = 0.014$, while the relative difference is $0.7\% < 1\%$ at $Bo = 0.007$. Therefore, the gravity should be considered when $Bo \geq 0.014$.

In addition, we carried out a large number of numerical simulations on the jumping behavior with numerous radii under different gravities to find out the general law of affecting the jumping behavior. Liu et al. (Liu et al. 2014b) analyzed the effects of gravity and drag force on the jumping process in Stage IV, which can be expressed as:

$$\mathbf{F}_g = \frac{8}{3}\rho_l \pi r^3 g,\ \mathbf{F}_d = 6\pi\mu_v\left(\sqrt[3]{2}R\right)v \tag{15}$$

where R is radius of coalesced droplet and v is the droplet velocity. Due to detaching from surface, viscous dissipation of the coalesced droplets is negligible in Stage IV. Therefore, comparing the relative magnitudes of gravity and drag force ($\mathbf{F}_g/\mathbf{F}_d$) can determine whether the gravity coefficient is considered in the jumping behavior. The droplet velocity (v) and gravitational coefficient (g) are represented by the characteristic speed ($v = \sqrt{1.24\sigma_{lv}/\rho_l r}$) and Bo number, respectively. The proportional relationship between Bo and $1/r^{0.5}$ is obtained by simplifying the formula. Our numerical results show that when the droplet radii are 48.6, 97.2, 145.8 and 194.4, the corresponding critical Bo numbers are 0.014, 0.011, 0.0076 and 0.0067, respectively (Fig. 6). By fitting the results, we conclude that the relationship between critical Bo number and droplet radius is $Bo > \sqrt{0.00764/r}$, which is in good agreement with our LB results. Hence, the gravity should be considered at $Bo > \sqrt{0.00764/r}$ in the process of coalescence-induced droplet jumping.

It is well known that energy conversion efficiency of coalesced droplet is extremely low, and is affected by various factors, such as viscous dissipation, gravitational potential energy and blocking work caused by contact angle hysteresis. Based on the energy conservation model, Wang et al. (Wang et al. 2017a) conducted a numerical study on energy conservation efficiency of coalesced droplet and found that the maximum energy conservation efficiency does not exceed 6.0% without gravity. For two identical droplets coalescence, released surface energy before and after coalescence is expressed as:

$$\Delta E_s = 2\pi\sigma_{lv}\left[2(1-\cos\theta) + (1-\varphi-\varphi\cos\theta_Y)\sin^2\theta - 1.26\left(2-3\cos\theta+\cos^3\theta\right)^{2/3}\right]r_1^2 \tag{16}$$

where $\theta_Y = 150.8°$ is Young's contact angle and $\theta = 166°$ is apparent contact angle. In this simulation, solid fraction is $\varphi = 1/7$ (φ denotes the ratio of width and spacing of micropillars). Energy conversion efficiency is defined as the ratio of effective kinetic energy to released surface energy:

$$\eta = \frac{E_k}{\Delta E_s} \times 100\% \tag{17}$$

The maximum vertical velocity is chosen to calculate the effective kinetic energy:

$$E_k = \frac{1}{2}mU_m^2 = \rho_l \times \frac{4}{3}\pi r^3 \times \left(v_{ym}^*\right)^2 \times \frac{\sigma_{lv}}{\rho_l r} = \frac{4}{3}\pi r^2\sigma_{lv} \times \left(v_{ym}^*\right)^2 \tag{18}$$

Substitute Eqs. 16 and 18 into Eq. 17, we obtain the energy conversion efficiency:

$$\eta = \frac{2\left(v_{ym}^*\right)^2 \times 100\%}{6(1-\cos\theta) + 3(1-\varphi-\varphi\cos\theta_Y)\sin^2\theta - 3.78(2-3\cos\theta+\cos^3\theta)^{2/3}} \tag{19}$$

Figure 7 shows the energy conversion efficiency of coalesced droplet under different *Bo* numbers (*Oh* = 0.017). It has been illustrated in Fig. 5 that gravity is

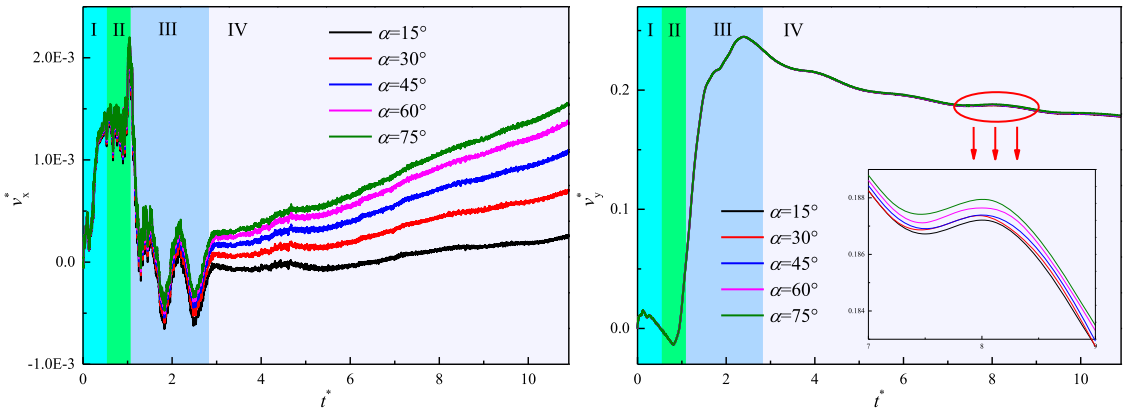

(a) g = 0.1×10^{-7}

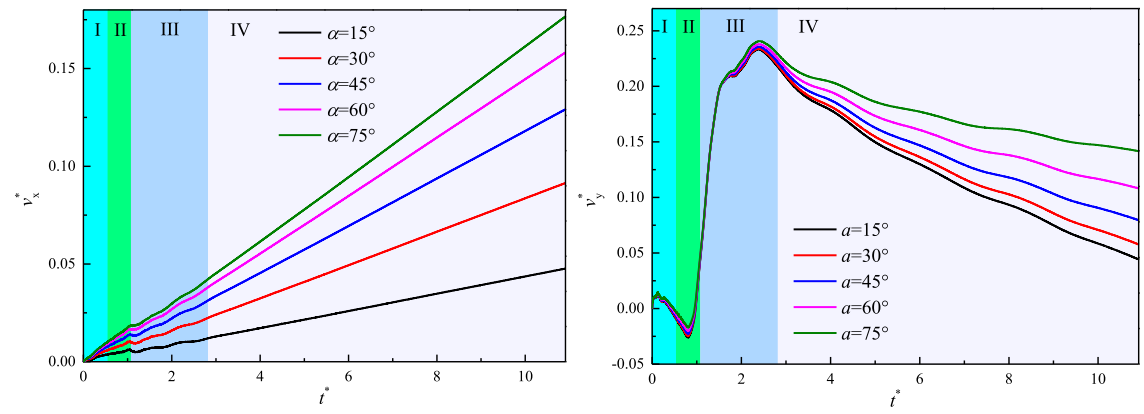

(b) g = 10×10^{-7}

Fig. 4 Variation of jumping velocity with time on different inclined surfaces (*Oh* = 0.017, $\theta = 166°$). (**a**) g = 0.1 × 10^{-7}, (**b**) g = 10 × 10^{-7}

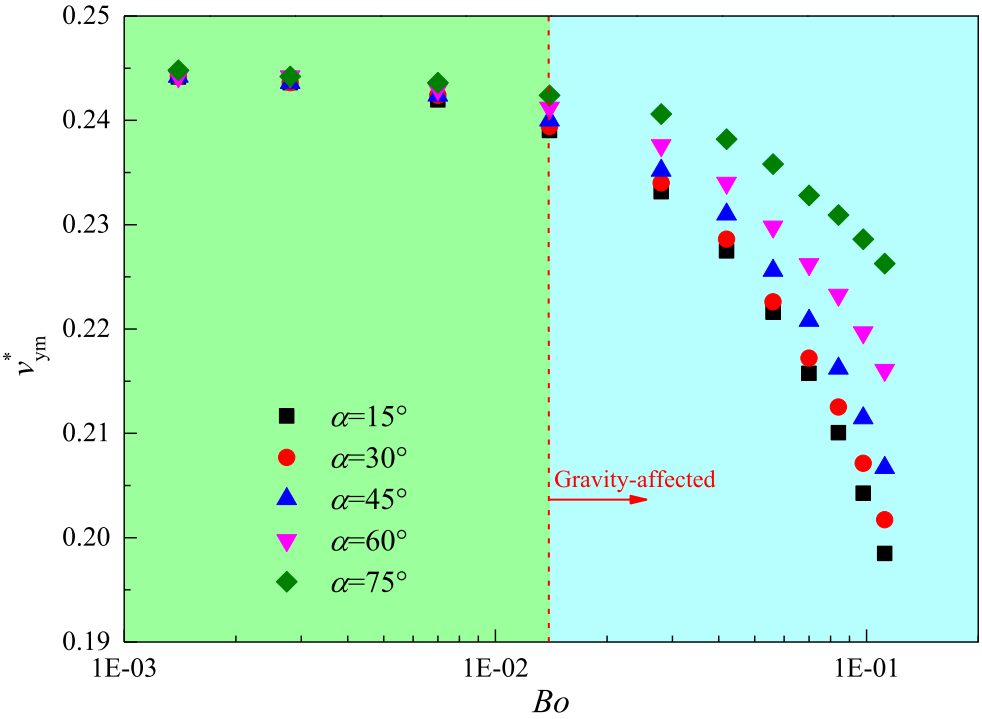

Fig. 5 Effect of *Bo* number (gravitational coefficient) on maximum vertical jumping velocity ($Oh = 0.017$, $\theta = 166°$)

considered when $Bo \geq 0.014$, therefore energy conversion efficiency at $Bo \geq 0.014$ is calculated. It can be seen from Fig. 7 that coalescence-induced jumping is an extremely inefficient process, with less than 5% of the released surface energy converted to the effective kinetic energy of droplet. As the Bo number increases, energy conversion efficiency drops significantly. The smaller the surface inclined angle, the faster the energy conversion efficiency decreases from 4.84% to 3.18%. The results demonstrate that gravity coefficient has a

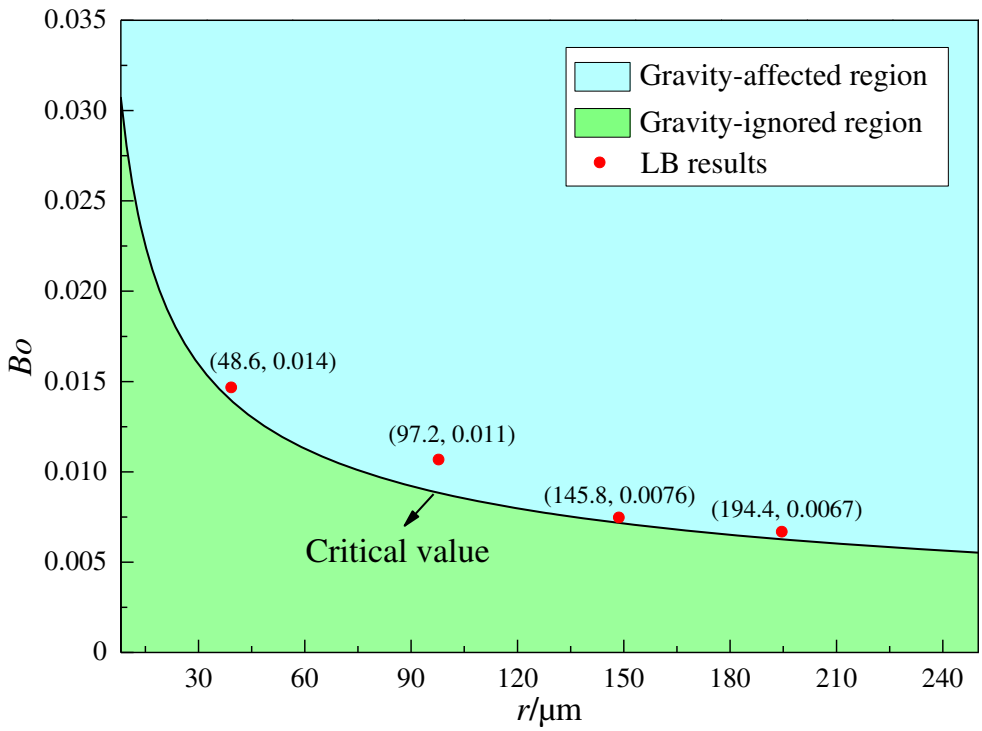

Fig. 6 Effect of *Bo* number on the jumping behavior

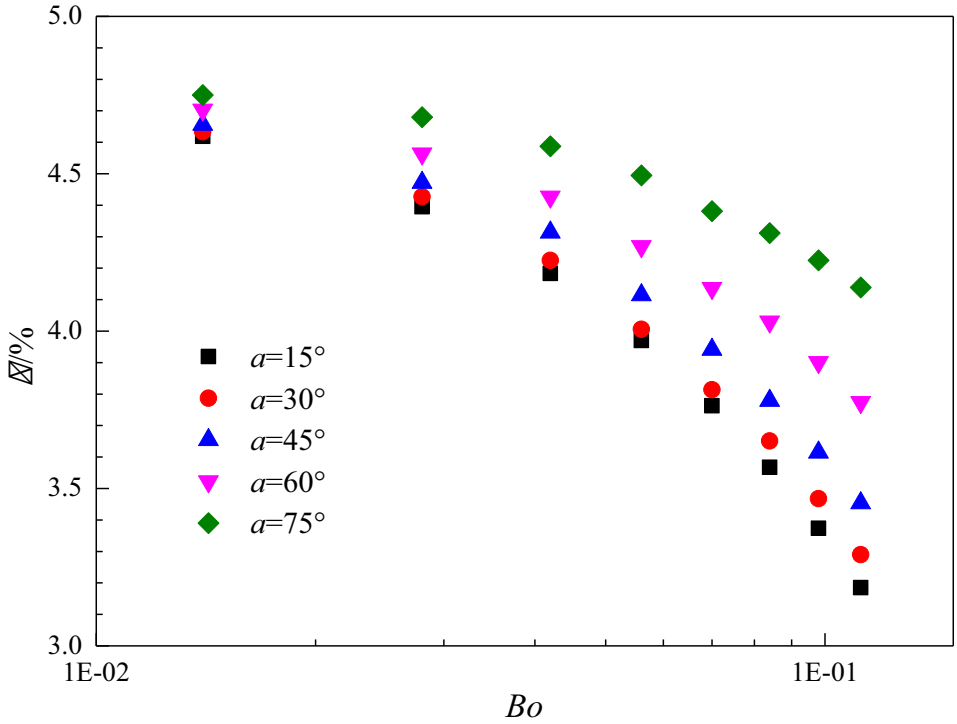

Fig. 7 Energy conversion efficiency of coalesced droplet under different *Bo* numbers ($Oh = 0.017$, $\theta = 166°$)

great influence on the energy conversion efficiency of coalesced droplet. A larger inclined angle greatly improves the conversion efficiency.

Two Mismatched Droplets

In section 4.1, jumping dynamics induced by two equal droplets coalescence is studied. However, coalesced droplets are not absolutely equal in most cases. Therefore, dynamic behaviors of two mismatched droplets coalescence-induced jumping are simulated, as shown in Fig. 8. ϕ is defined as the radius ratio of the smaller droplet to the larger droplet ($\phi = r_s/r_l$). Since the dimensionless inertia-capillary time is related to the coalesced droplet radius, inertial-capillary time is calculated using the larger droplet radius. As can be found from Fig. 8, the jumping dynamics of two mismatched droplets can also be divided into four stages, whereas it is different from two-identical droplets jumping dynamics. The time of liquid bridge formation is significantly reduced because expansion of liquid bridge is limited by the smaller droplets. Due to the asymmetry of merged droplet, the left side of droplet first impacts the wall. Compared with two-identical droplets coalescence (Fig. 3), two-mismatched droplets jump off the surface earlier at $t^* = 2.4$. It is worth noting that two-mismatched droplets coalesce to produce a tangential driving force, resulting in a certain displacement relative to the solid surface. Moreover, the jumping velocity and height are decreased as a result of the reduction in released surface energy.

In order to eliminate the influence of gravity on the tangential jumping velocity, variation of jumping velocities of coalesced droplets on horizontal surfaces with time is investigated. As mentioned earlier, dimensionless inertia-capillary time is related to the droplet radius. The larger radius of droplet is chosen to calculate inertia-capillary time and *Oh* number. Figure 9 shows variation of jumping velocities with time at constant *Oh* number ($Oh = 0.017$). At the early stage of coalescence (liquid bridge formation), the larger droplet engulf the smaller one, resulting in moving along the horizontal direction (corresponding to the increase in horizontal velocity

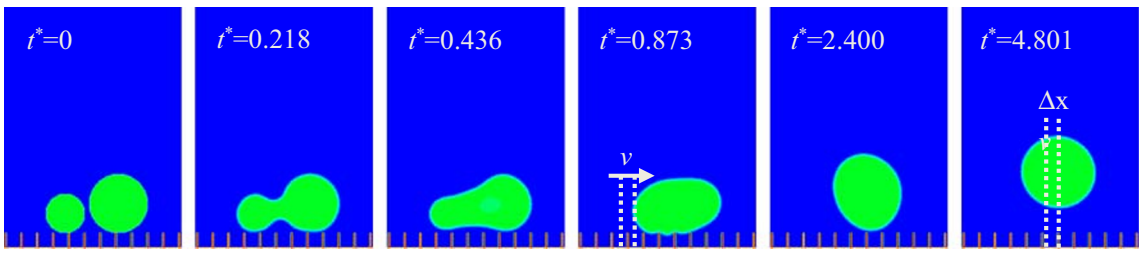

Fig. 8 Dynamic behavior of coalescence-induced two mismatched droplets jumping ($Oh = 0.017$, $\phi = 0.67$)

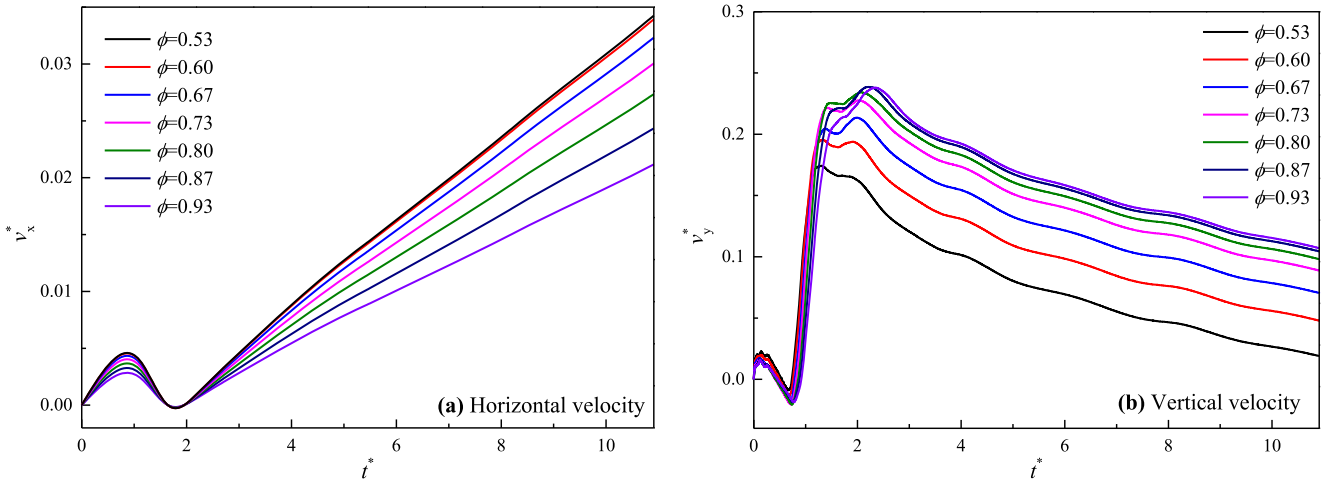

Fig. 9 Variation of jumping velocity with time ($Oh = 0.017$). (**a**) Horizontal velocity, (**b**) Vertical velocity

from $t^* = 0$ to $t^* = 0.873$). In this stage, liquid bridge expands to impact the solid substrate and vertical velocity is reduced to a minimum. Subsequently, horizontal velocity decreases wit time from $t^* = 0.873$ to $t^* = 1.8$ (Stage III, retraction), while vertical velocity increases rapidly with time. The smaller the radius ratio, the lower the maximum velocity of coalesced droplet is. It is worth noting that there are two peak velocities during two mismatched droplets merging. As the radius ratio increases, the maximum vertical velocity changes from the first peak velocity to the second one. And the time of maximum velocity appearing is pushed back. In stage IV (detaching from the surface), horizontal velocity increases linearly with time. Vertical velocity decreases with time due to the effect of gravity and drag force, but the decrease rate is independent of the radius ratio. Figure 10 shows the change of droplet velocity with time at different *Oh* numbers. The change of horizontal velocity is similar to Fig. 9(a). Nevertheless, as the *Oh* number decreases, each stage of coalesced droplet experiences a shorter time. At the early time, horizontal velocity increases with time, while vertical velocity decreases with time caused by the liquid bridge expanding and hitting the solid wall. During retraction and detachment from the surface, horizontal velocity decreases and then increases with time, bringing about the displacement along x direction. The maximum vertical velocity decreases with a smaller radius ratio because a smaller radius ratio increases the energy dissipation. The numerical results demonstrate that coalesced droplets can be swept away or merge with other drops after two-mismatched droplets coalescence. Although the smaller radius ratio reduces the maximum vertical velocity, horizontal velocity can be increased to achieve a better sweeping effect.

Figure 11 shows the effect of gravity on maximum jumping velocity and energy conversion efficiency at the constant *Oh* number ($r_1 = 48.6$ μm). For the same *Bo* number, maximum jumping velocity increases as the radius ratio increases, but the increase rate is

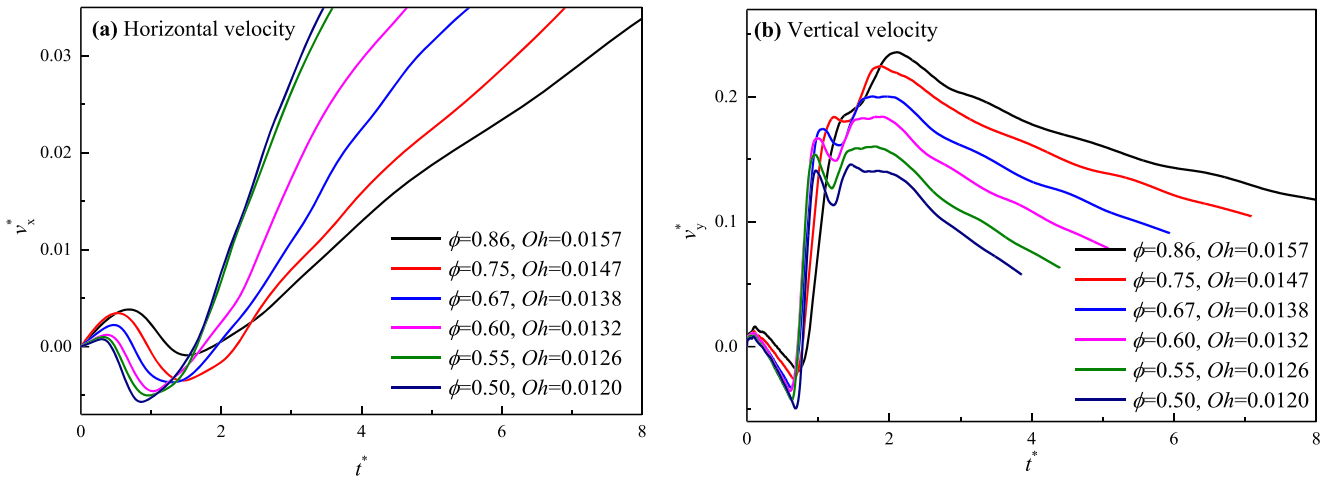

Fig. 10 Variation of jumping velocity with time at different *Oh* numbers. (**a**) Horizontal velocity, (**b**) Vertical velocity

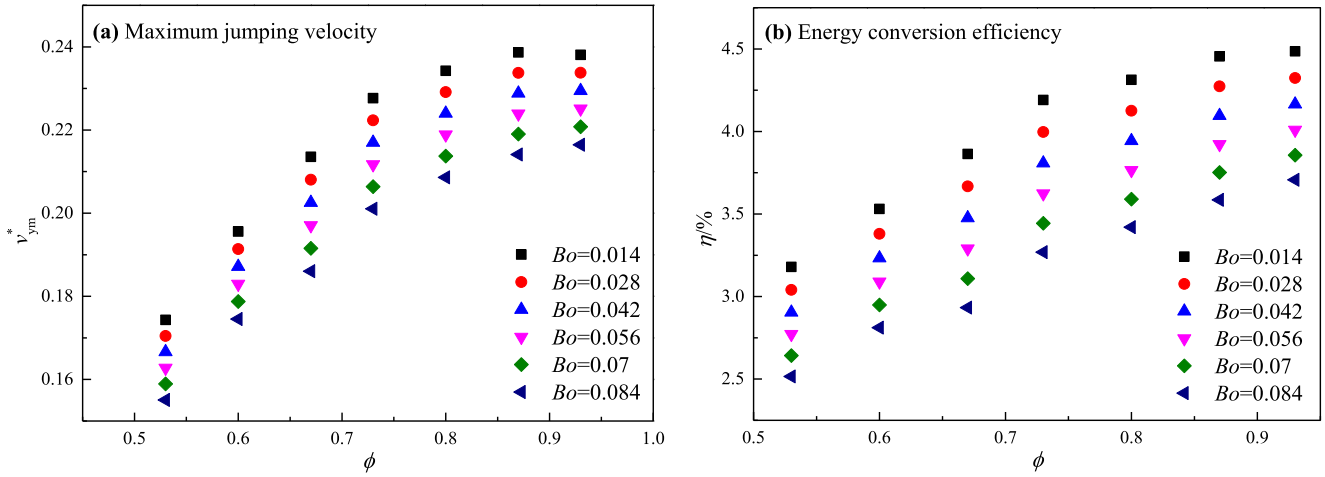

Fig. 11 Effect of gravity on maximum jumping velocity and energy conversion efficiency at the constant *Oh* number

reduced gradually. 35% growing rate of maximum jumping velocity can be seen as the radius ratio increases from 0.53 to 0.93. With the increase of *Bo* number, maximum jumping velocity of droplet with the same radius is reduced by 10% approximately. Compared with influence of the radius ratio on maximum jumping velocity, *Bo* number has little effect but cannot be ignored. Since the merged larger-droplet radii are unequal, Eq. 19 is no longer suitable for calculating energy conversion efficiency. Energy conversion efficiency after two mismatched droplets coalescence is reanalyzed. The initial surface energy of coalesced droplet is:

$$E_i = \sigma_{lv}\pi\left[2(1-\cos\theta) + (1-\varphi-\varphi\cos\theta_Y)\sin^2\theta\right]r_1^2\left(1+\phi^2\right) + \sigma_{sv}A_{total} \quad (20)$$

where σ_{lv} is the interface energy between solid and liquid and A_{total} is the total surface area. The final surface energy of coalesced droplet is as follows:

$$E_f = 4\sigma_{lv}\pi r_1^2\left[\frac{\left(1+\phi^3\right)\times\left(2-3\cos\theta+\cos^3\theta\right)}{4}\right]^{2/3} + \sigma_{sv}A_{total} \quad (21)$$

The released surface energy before and after coalescence is obtained by Eq.20 minus Eq. 21:

$$\Delta E_s = \pi\sigma_{lv}\{\left(1+\phi^2\right)\times\left[2(1-\cos\theta)+(1-\varphi-\varphi\cos\theta_Y)\sin^2\theta\right] - \left(1+\phi^3\right)^{2/3}\times\left(4-6\cos\theta+2\cos^3\theta\right)^{2/3}\}r_1^2 \quad (22)$$

It is found that Eq. 22 can be transformed into Eq. 16 for $\phi = 1$ ($r_s = r_1$). And energy conversion efficiency of two mismatched droplets is given by:

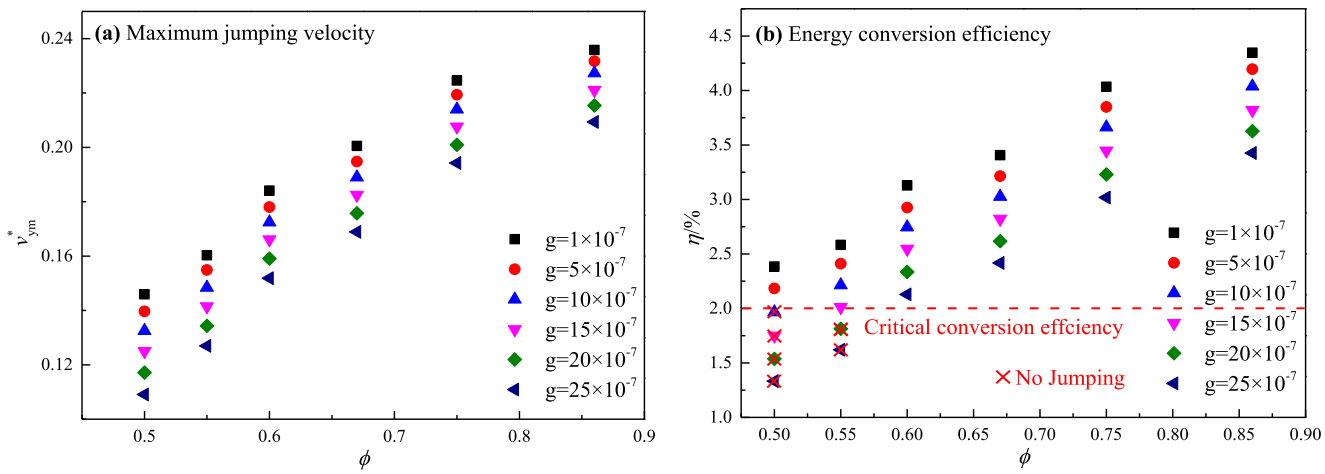

Fig. 12 Effect of gravity on maximum jumping velocity and energy conversion efficiency at different *Oh* numbers

$$\eta = \frac{\left(1+\phi^3\right)\times\left(2-3\cos\theta+\cos^3\theta\right)}{6\left[\left(1+\phi^2\right)\times\left(2(1-\cos\theta)+(1-\varphi-\varphi\cos\theta_Y)\sin^2\theta\right)-\left(1+\phi^3\right)^{2/3}\times\left(4-6\cos\theta+2\cos^3\theta\right)^{2/3}\right]}\left(v_{ym}^*\right)^2 \tag{23}$$

Figure 11(b) shows the corresponding energy conversion efficiency calculated by Eq. 23. Energy conversion efficiency is extremely low and less than 4.5%. Increasing the radius ratio has a positive effect on energy conversion efficiency, whereas a larger *Bo* number reduces it. When the radius ratio increases from 0.53 to 0.93, energy conversion efficiency can be improved by more than 40%, while it decreases by 20% with the *Bo* number from 0.014 to 0.084.

Figure 12 shows the effect of gravity on maximum jumping velocity and energy conversion efficiency at different *Oh* numbers. Due to the *Bo* number related to both droplet radius and gravitational coefficient, effect of gravity cannot be expressed by *Bo* number at different *Oh* numbers. For the same radius ratio, v_{ym}^* and η are reduced by more than 11% and 21% respectively as gravitational coefficient increases from 1×10^{-7} to 25×10^{-7}. For the same gravitational coefficient, v_{ym}^* and η can be significantly increased by 38% and 45% as the radius ratio increases from 0.5 to 0.86. In addition, η is less than 2.0% and no-jumping behavior of coalesced droplets can be seen at a larger gravitational coefficient and a smaller radius ratio (larger *Oh* number).

Conclusion

Coalescence-induced droplet jumping dynamics (two-identical droplets and two-mismatched droplets) on superhydrophobic surfaces with micropillar arrays is simulated using the lattice Boltzmann method. Effects of gravitational coefficient, surface orientation and radius ratio of coalesced droplets on the jumping velocity and energy conversion efficiency are analyzed. Several conclusions can be summarized as follows.

(1) coalescence-induced droplet jumping can be divided into four stages: (I) liquid bridge formation after coalescence; (II) liquid bridge expanding and impacting the solid substrate; (III) retraction caused by the wall reaction and (IV) jumping off the surface. Compared with identical droplets coalescence, time of liquid bridge formation of mismatched droplets merging in Stage (I) is significantly reduced, which is because liquid bridge expanding is limited by the smaller coalesced droplet.

(2) For two-identical droplets coalescence, jumping droplets on the inclined surface driven by the tangential gravity can successfully detach from the surface without returning to the original spot. A larger inclined angle has a positive impact on the jumping dynamics. Effect of gravitational force on the jumping behavior of coalesced droplet should be considered when $Bo > \sqrt{0.00764/r_1}$.

(3) Coalescence-induced jumping of two-mismatched droplets can produce a horizontal velocity that drives them detaching from the surface or coalescing with other droplets. Furthermore, jumping velocity and energy conversion efficiency are reduced by a lower radius ratio and a larger gravitational coefficient. It should be noted that no jumping occurs when energy conversion efficiency is less than 2%.

Acknowledgments This work was supported by ESA-CMSA International Cooperation of Space Experiment Project (Study on Condensation and Enhancement Methods under Microgravity) and the Scientific Research Foundation of Graduate School of Southeast University (YBPY1949).

References

Barthlott, W., Neinhuis, C.: Purity of the sacred lotus, or escape from contamination in biological surfaces. Planta. **202**, 1–8 (1997)

Boreyko, J.B., Chen, C.: Self-propelled dropwise condensate on superhydrophobic surfaces. Phys. Rev. Lett. **103**, 184501 (2009)

Boreyko, J.B., Collier, C.P.: Delayed frost growth on jumping-drop superhydrophobic surfaces. ACS Nano. **7**, 1618–1627 (2013)

Cha, H., Xu, C., Sotelo, J., Chun, J.M., Yokoyama, Y., Enright, R., Miljkovic, N.: Coalescence-induced nanodroplet jumping. Phys. Rev. Fluids. **1**, 064102 (2016)

Chen, Y., Deng, Z.: Hydrodynamics of a droplet passing through a microfluidic T-junction. J. Fluid Mech. **819**, 401–434 (2017)

Cheng, Y., Xu, J., Sui, Y.: Numerical investigation of coalescence-induced droplet jumping on superhydrophobic surfaces for efficient dropwise condensation heat transfer. Int. J. Heat Mass Tran. **95**, 506–516 (2016)

Chu, F., Wu, X., Wang, L.: Dynamic melting of freezing droplets on ultraslippery superhydrophobic surfaces. ACS Appl. Mater. Inter. **9**, 8420–8425 (2017)

Farokhirad, S., Morris, J.F., Lee, T.H.: Coalescence-induced jumping of droplet: inertia and viscosity effects. Phys. Fluids. **27**, 102102 (2015)

Gong, S., Cheng, P.: Numerical investigation of droplet motion and coalescence by an improved lattice Boltzmann model for phase transitions and multiphase flows. Comput. Fluids. **53**, 93–104 (2012)

Hou, Y., Yu, M., Shang, Y., Zhou, P., Song, R., Xu, X., Chen, X., Wang, Z., Yao, S.: Suppressing ice nucleation of supercooled condensate with biphilic topography. Phys. Rev. Lett. **120**, 075902 (2018)

Khatir, Z., Kubiak, K.J., Jimack, P.K., Mathia, T.G.: Dropwise condensation heat transfer process optimisation on superhydrophobic surfaces using a multi-disciplinary approach. Appl. Therm. Eng. **106**, 1337–1344 (2016)

Kim, M.K., Cha, H., Birbarah, P., Chavan, S., Zhong, C., Xu, Y., Miljkovic, N.: Enhanced jumping-droplet departure. Langmuir. **31**, 13452–13466 (2015)

Li, Q., Kang, Q., Francois, M.M., Hu, A.: Lattice Boltzmann modeling of self-propelled Leidenfrost droplets on ratchet surfaces. Soft Matter. **12**, 302–312 (2016)

Liu, X., Cheng, P.: 3D multiphase lattice Boltzmann simulations for morphological effects on self-propelled jumping of droplets on textured superhydrophobic surfaces. Int. J. Commun. Heat Mass. **64**, 7–13 (2015)

Liu, F., Ghigliotti, G., Feng, J., Chen, C.: Numerical simulations of self-propelled jumping upon drop coalescence on non-wetting surfaces. J. Fluid Mech. **752**, 39–65 (2014a)

Liu, X., Cheng, P., Quan, X.: Lattice Boltzmann simulations for self-propelled jumping of droplets after coalescence on a superhydrophobic surface. Int. J. Heat Mass Tran. **73**, 195–200 (2014b)

Miljkovic, N., Enright, R., Nam, Y., Lopez, K., Dou, N., Sack, J., Wang, E.N.: Jumping-droplet-enhanced condensation on scalable superhydrophobic nanostructured surfaces. Nano Lett. **13**, 179–187 (2013)

Mukherjee, R., Berrier, A.S., Murphy, K.R., Vieitez, J.R., Boreyko, J.B.: How surface orientation affects jumping-droplet condensation. Joule. **3**, 1–17 (2019)

Shi, Y., Tang, G., Xia, H.: Investigation of coalescence-induced droplet jumping on superhydrophobic surfaces and liquid condensate adhesion on slit and plain fins. Int. J. Heat Mass Tran. **88**, 445–455 (2015)

Shi, J., Ma, Q., Chen, Z.: Numerical study on bubble motion in pore structure under microgravity using the lattice Boltzmann method. Microgravity Sci. Tec. **31**, 207–222 (2019)

Wang, K., Li, R., Liang, Q., Jiang, R., Jiang, Y., Lan, Z., Ma, X.: Critical size ratio for coalescence-induced droplet jumping on superhydrophobic surfaces. Appl. Phys. Lett. **111**, 061603 (2017a)

Wang, K., Liang, Q., Jiang, R., Zheng, Y., Lan, Z., Ma, X.: Numerical simulation of coalescence-induced jumping of multidroplets on superhydrophobic surfaces: initial droplet arrangement effect. Langmuir. **33**, 6258–6268 (2017b)

Wang, J., Gao, W., Zhang, H., Zou, M., Chen, Y., Zhao, Y.: Programmable wettability on photocontrolled graphene film. Sci. Adv. **4**, eaat7392 (2018a)

Wang, K., Liang, Q., Jiang, R., Zheng, Y., Lan, Z., Ma, X.: Morphology evolution and dynamics of droplet coalescence on superhydrophobic surfaces. AICHE J. **64**, 2913–2921 (2018b)

Wang, X., Chen, Z., Xu, B.: Coalescence-induced jumping of condensate droplets on microstructured surfaces with different gravitational fields by lattice Boltzmann method. Comput. Fluids. **188**, 60–69 (2019)

Wang, X., Xu, B., Chen, Z., Yang, Y., Cao, Q.: Lattice Boltzmann modeling of condensation heat transfer on downward-facing surfaces with different wettabilities. Langmuir. **36**, 9204–9214 (2020)

Wen, R., Xu, S., Ma, X., Lee, Y.C., Yang, R.: Three-dimensional superhydrophobic nanowire networks for enhancing condensation heat transfer. Joule. **2**, 269–279 (2018)

Wen, R., Zhou, X., Peng, B., Lan, Z., Yang, R., Ma, X.: Falling-droplet-enhanced filmwise condensation in the presence of non-condensable gas. Int. J. Heat Mass Tran. **140**, 173–186 (2019)

Wisdom, K.M., Watson, J.A., Qu, X., Liu, F., Watson, G.S., Chen, C.: Self-cleaning of superhydrophobic surfaces by self-propelled jumping condensate. P. Natl. Acad. Sci. **110**, 7992–7997 (2013)

Xie, H., Zeng, Z., Zhang, L., Yokota, Y., Kawazoe, Y., Yoshikawa, A.: Simulation on thermocapillary-driven drop coalescence by hybrid lattice Boltzmann method. Microgravity Sci. Tec. **28**, 67–77 (2016)

Xie, J., Xu, J., Li, X., Liu, H.: Dropwise condensation on superhydrophobic nanostructure surface, part I: long-term operation and nanostructure failure. Int. J. Heat Mass Tran. **129**, 86–95 (2019)

Xu, B., Chen, Z.: Droplet movement on a composite wedge-shaped surface with multi-gradients and different gravitational field by molecular dynamics. Microgravity Sci. Tec. **30**, 571–579 (2018)

Xu, B., Chen, Z.: Condensation on composite V-shaped surface with different gravity in nanoscale. Microgravity Sci. Tec. **31**, 603–613 (2019)

Xu, Q., Li, J., Tian, J., Zhu, J., Gao, X.: Energy-effective frost-free coatings based on superhydrophobic aligned nanocones. ACS Appl. Mater. Inter. **6**, 8976–8980 (2014)

Yan, X., Zhang, L., Sett, S., Feng, L., Zhao, C., Huang, Z., Vahabi, H., Kota, A.K., Chen, F., Miljkovic, N.: Droplet jumping: effects of droplet size, surface structure, pinning, and liquid properties. ACS Nano. **13**, 1309–1323 (2019)

Yuan, Z., Wu, X., Chu, F., Wu, R.: Numerical simulations of guided self-propelled jumping of droplets on a wettability gradient surface. Appl. Therm. Eng. **156**, 524–530 (2019)

Zhang, J., Liu, H., Ba, Y.: Numerical study of droplet dynamics on a solid surface with insoluble surfactants. Langmuir. **35**, 7858–7870 (2019)